Etalon@lateral flow strip for integrated separation-sensing microfluidic platforms

Zhang, Mengmeng; Loeve, Arjo J.; Serpe, Michael J.; Bazyar, Hanieh

DOI
10.1016/j.bios.2025.117656

Publication date
2025

Document Version
Final published version

Published in
Biosensors and Bioelectronics

Citation (APA)
Zhang, M., Loeve, A. J., Serpe, M. J., & Bazyar, H. (2025). Etalon@lateral flow strip for integrated separation-sensing microfluidic platforms. *Biosensors and Bioelectronics*, *287*, Article 117656. https://doi.org/10.1016/j.bios.2025.117656

Biosensors and Bioelectronics 287 (2025) 117656

Contents lists available at ScienceDirect

Biosensors and Bioelectronics

journal homepage: www.elsevier.com/locate/bios

Etalon@lateral flow strip for integrated separation-sensing microfluidic platforms

Mengmeng Zhang [a], Arjo J. Loeve [b,c], Michael J. Serpe [d], Hanieh Bazyar [e,*]

[a] Department of Process & Energy, Delft University of Technology, Leeghwaterstraat 39, Delft, 2628 CB, The Netherlands
[b] Department of BioMechanical Engineering, Delft University of Technology, Mekelweg 2, Delft, 2628 CD, The Netherlands
[c] Co van Ledden Hulsebosch - Netherlands Center for Forensic Science and Medicine, Science Park – Building 904, Amsterdam, 1098 XH, The Netherlands
[d] Department of Chemistry, University of Alberta, 11227 Saskatchewan, Edmonton, T6G 2G2, Canada
[e] Department of Chemical Engineering, Delft University of Technology, Van der Maasweg 9, Delft, 2629 HZ, The Netherlands

ARTICLE INFO

Keywords:
Etalon
Lateral flow assays
Commercial membranes
Integrated separation-sensing platform
Microfluidics

ABSTRACT

Lateral flow assays (LFAs) are widely favored for on-site analysis due to their simplicity and cost-effectiveness. However, their limited quantitative capabilities constrain them to qualitative testing. In contrast, etalon sensors offer high sensitivity and enable quantitative detection. They operate by producing interference-based optical signals through multiple reflections of light within a cavity formed by two parallel reflective surfaces. This requires a stable optical path length, traditionally limiting their use to smooth substrates.

This study presents an integrated separation-sensing microfluidic platform (EtLFA). By fabricating etalons on commercial membranes and evaluating sensor's sensitivity and surface roughness, we determined that membrane surface roughness must meet two criteria — Sa < 0.5 μm and Smr > 90% — to support functional etalons. Capillary and permeability remain intact after etalon integration, ensuring membrane's purification performance. We further functionalized the etalon to respond specifically to glucose, to demonstrate the quantitative detection of glucose levels in a mimic blood sample. A glucose-responsive etalon@nylon served as the sensor module, while regenerated cellulose membrane enabled separation. This dual-module configuration filtered PDMS particles mimicking red blood cells and produced a 25 nm shift for 100 mg/dL glucose, enabling linear quantification via portable spectrometry. By incorporating etalon sensor onto rough membrane substrates, our platform transforms conventional LFAs into a quantitative analytical tool, offering novel avenues for enhancing analytical capabilities and broadening the applications of lateral flow assays.

1. Introduction

Lateral flow assays (LFAs) are widely employed in paper-based point-of-care (POC) devices, renowned for their affordability, speed, and simplicity in on-site bioanalytical targets analysis and quantification (Gubala et al., 2012). Initially utilized for detecting human chorionic gonadotropin hormone in urine for pregnancy tests, LFAs have expanded their utility to encompass a diverse array of analytes, including disease biomarkers (Gumus et al., 2023), DNA (Zheng et al., 2021), toxins (İnce et al., 2023), and microbiomes (Fuentes-Chust et al., 2021). In recent decades, LFAs have demonstrated remarkable versatility, finding applications across various fields such as medical diagnostics (Sadeghi et al., 2021; Zhou et al., 2021), environmental monitoring (Jara et al., 2022), and food safety (Younes et al., 2023).

The LFAs have been the hero of the COVID-19 pandemic by enabling self-testing, fast read-out, and decentralized health diagnosis (Budd et al., 2023). They are composed of four distinct components: a sample pad, a conjugate pad, a detection pad, and an absorbent pad, all housed within a plastic backing card (Mark et al., 2010). The operating principle of LFAs involves the absorption of a liquid sample containing the analyte by the sample pad, followed by its migration through the conjugate pad, where analyte-interacting molecules, typically detection antibodies conjugated with visible labels, are attached. The sample, along with these labeled biorecognition elements proceeds to the detection zone, which is typically a nitrocellulose membrane. Here, capture bioreceptors are immobilized at defined positions to form the test and control lines. Upon interaction with the analyte, the conjugated complexes bind to these immobilized receptors, generating visible signals at the respective line. LFAs offer notable advantages, including ease of use, compatibility with small sample volumes, and in many cases, long-term stability without refrigeration. Furthermore, their functionality can be enhanced by integration with onboard electronics and information systems for streamlined data analysis.

* Corresponding author.
E-mail addresses: m.zhang-7@tudelft.nl (M. Zhang), A.J.Loeve@tudelft.nl (A.J. Loeve), serpe@ualberta.ca (M.J. Serpe), h.bazyar@tudelft.nl (H. Bazyar).

https://doi.org/10.1016/j.bios.2025.117656
Received 7 January 2025; Received in revised form 26 May 2025; Accepted 2 June 2025
Available online 18 June 2025

Based on the aforementioned structure and operation, LFAs can be classified into two main assay types: non-competitive (sandwich) and competitive assays (Davies, 2013). In the non-competitive assay, the intensity of the test line proportionally increases with the concentration of the target analyte, while it is vice versa in the competitive assays. This makes competitive assays a suitable method to detect small molecules. Over the years, extensive reviews have explored the development (Singh et al., 2023) design (Dey et al., 2023). In a recent review by Pedreira-Rincón et al. (2025), the design, optimization strategies for different components, and corresponding applications of the competitive LFAs have been comprehensively reviewed. The mathematical modeling of this type of LFAs have been investigated in detail, demonstrating the advantage of theoretical modeling to optimize LFAs in a fast and less expensive manner, eliminating the need for extensive experiments.

In the review by Budd et al. (2023) pathways to increase sensitivity and specificity of LFAs have been detailed to develop next-generation LFAs for various disease diagnosis, spanning infectious diseases to cancers. Possible scenarios such as implementing emerging materials e.g., nano- and quantum-dots to improve sensitivity, and nucleic acid amplification to increase specificity have been investigated. Additionally, the role of deep learning approaches to achieve digital LFAs has been discussed in detail, enabling widespread self-testing and decentralized diagnosis.

A wide range of other approaches to increase LFAs' sensitivity and specificity have been reviewed by Kakkar et al. (2024). Integrating analytical techniques, e.g., optical, fluorescence, electrochemical, photoacoustics, polymerase chain reaction (PCR), and Raman scattering have been detailed. These techniques can further increase the limits of detection, enabling multiplexing. Implementing new recognition elements, namely, aptamers and molecularly imprinted polymers (synthetic receptors for targeted molecules) can improve the LFA's specificity. These enhancements pave the way for LFAs' wide-spread application spanning agriculture and food, environmental monitoring, and human as well as animal health.

A novel and sustainable approach to increase LFAs' limit of detection and analytical sensitivity is including flow constraints in the detection pad (nitrocellulose membrane). This enables longer specific binding interactions between the analyte and the labeled antibody. Khatmi et al. studied such flow constraints by structuring the nitrocellulose membrane with vertical micro channels (Khatmi et al., 2024). These channels were micromachined using femtosecond laser cold ablation and the influence of the channel width and density were investigated. This flow rate delaying approach showed 40% increase in the signal sensitivity of the colorimetric readout to detect SARS-CoV-2 analyte compared with the untreated pristine LFA.

A significant challenge in conventional LFAs lies in their inability to extensively purify or separate complex clinical samples such as whole blood. Although various membranes, such as the sample pad, conjugate pad, detection pad, and absorption pad, are integrated into LFA designs, their primary functions are typically sample conditioning and reagent delivery rather than extensive purification or separation. For example, the sample pad may treat samples by adjusting properties like viscosity or pH to aid flow, while the conjugate pad facilitates the binding of labeled detection reagents to the target analytes. Nitrocellulose is commonly used for the detection pad due to its ability to immobilize biomolecules directly (Tang et al., 2022), but not inherently designed for extensive sample purification or separation. To address this, some commercial LFAs employ integrated separation membranes (Sena-Torralba et al., 2022), such as CytoSep® and Vivid™, that can passively remove red blood cells without off-chip processing.

Additionally, LFAs primarily provide qualitative or low-resolution semi-quantitative results (Koczula and Gallotta, 2016). This means they often deliver a binary indication of the presence or absence of an analyte rather than precise measurements of its concentration. The majority of commercially available LFAs are designed for qualitative or semi-quantitative analysis, requiring specialized equipment for accurate quantitative measurement of biomarkers (Dey et al., 2023). This poses extra challenges in scenarios where analyte concentration is crucial to determine, such as in medical diagnostics, environmental monitoring, and forensic analysis, where quantitative results can be paramount for decision-making.

In recent years, a novel type of optical sensor known as etalon, based on stimuli-responsive materials, e.g., poly(N-isopropylacrylamide) (PNIPAM) microspheres has been widely introduced and applied in the sensor field (Lanzalaco et al., 2023). These etalon sensors are constructed by sandwiching a thin layer of PNIPAM between two highly reflective metal films to form an optical cavity. PNIPAM exhibits unique properties, undergoing reversible volume phase transitions in response to temperature, pH levels, and various chemicals through copolymerization with functional groups (Lanzalaco et al., 2023; Lee et al., 2012; Maekawa et al., 2021; Shaibie et al., 2023). When subjected to sensing these targets, the volume of PNIPAM changes, altering the distance between the two reflective metal films, and generating shifts in the wavelength of the input light (optical spectrum).

The ability of PNIPAM to bind effectively with antibodies makes it a promising material for quantitative diagnostic tools (Wei et al., 2019; Herrmann et al., 2021; Das et al., 2024). A representative demonstration of PNIPAM-based etalon sensing capabilities is the steroid hormone detection system developed by Jiang et al. (2016). This sensor utilized a layer of PNIPAM microgel functionalized with specific antibodies, producing an optical response with visual color and multi-peak reflectance spectra. The sensor demonstrated a remarkably low detection threshold of 0.28 ng/mL, significantly lower than the proposed cut-off around 0.70 ng/mL (Venetis and Tarlatzis, 2018). Beyond antibodies, PNIPAM has also been functionalized with nucleic acid probes (Li et al., 2016; Guo et al., 2014; Du et al., 2023), aptamers (Xuan et al., 2016; Liu et al., 2024; Jiang et al., 2018), and enzymes (Chen and Hoffman, 1994; Cao and Wang, 2016), enabling detection of diverse analytes including biomacromoleculess such as IgG (Shen et al., 2023) and small molecules like glucose (Nam et al., 2023) and dopamine (Wang et al., 2021). These prior works lay the foundation for expanding our membrane-integrated etalon platform toward broader biosensing applications.

In this study, we introduce an etalon@lateral flow assay integrated separation-sensing microfluidic platform (EtLFA). This platform comprises two modules instead of the traditional four: a separation module and a sensing module. The EtLFA configuration is schematically shown in Fig. 1 while the assembly steps in Fig. 6a. The etalon@membrane (sensing module) is positioned at the edge of the separation membrane, allowing for analyte detection following separation. For the separation module, instead of developing new membrane materials, we employ commercially available membranes without the need for external sample pre-processing. The sensing module is created by coating etalons, fabricated from temperature-responsive PNIPAM sandwiched between two gold layers (gold/PNIPAM/gold), onto these commercial membranes. As far as we are aware, this represents the first investigation to explore etalon functionality on a rough surface such as a polymeric porous membrane. Through surface roughness analysis, wicking, and permeance measurements, we investigated the interplay between membrane properties and the etalon's optical and fluidic behavior, establishing practical criteria for selecting membranes suitable for etalon fabrication. Additionally, we demonstrated the system's utility by developing a glucose-responsive EtLFA, showcasing its enhanced analytical capabilities and potential to expand the applications of lateral flow assays. This research opens the possibility of integrating etalon and LFA technologies, enabling both complex sample purification and analyte quantification in a rapid, on-site manner. This dual capability is especially beneficial for applications in clinical diagnostics, forensic analysis, and environmental testing, where precise separation and measurement are essential.

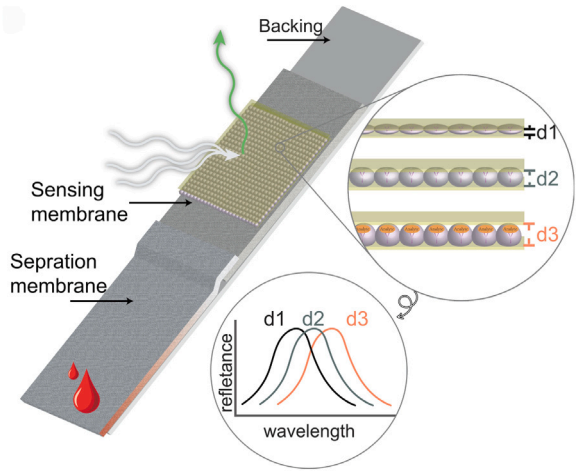

Fig. 1. The schematic configuration of the etalon@lateral flow assay microfluidic platforms (EtLFA) consists of two components: the separation module and the sensing module. The separation module utilizes a commercial membrane, while the sensing module features a membrane coated with an etalon—a sandwich structure composed of two gold layers encapsulating a monolithic micro-bead layer made of Poly(N-isopropyl acrylamide). This Poly(N-isopropyl acrylamide) can be modified to couple with specific target analytes. When the target analyte binds to the modified polymer, the resulting increase in volume causes a peak shift in the reflectance spectrum, which can serve as a quantitative index of the analyte concentration. The variables d_1, d_2, and d_3 indicate different distances between the two gold layers under varying conditions, corresponding to changes in analyte concentration.

2. Experimental setup

2.1. Membranes exploration for sensing module

2.1.1. Membranes

The commercial membranes used in this study were track-etched polycarbonate membrane, abbreviated as TE-PC (Whatman® Nuclepore™ Track-Etched Membranes, diameter 25 mm, pore size 0.20 μm), nylon membrane (Nylaflo™, Pall Lab, diameter 47 mm, pore size 0.20 μm), regenerated cellulose membrane, abbreviated as RC (Sartorius, type 18,407, diameter 47 mm, 0.20 μm pore size), polyethersulfone, abbreviated as PES (Millipore® Express PLUS GPWP04700, diameter 47 mm, 0.22 μm pore size), nitrocellulose membrane, abbreviated as NC (Millipore® Z358657, diameter 293 mm, 0.22 μm pore size), and glass fiber membrane, abbreviated as GF (Millipore® Binder Resin Glass Fiber AP2002500, diameter 25 mm, 2.0 μm pore size). All the membranes were hydrophilic and used without any pre-processing unless otherwise stated.

2.1.2. Fabrication of sensing module

The sensing module was fabricated by coating an etalon structure on commercial membranes. The procedure was as described in the literature (Sorrell et al., 2011) and is summarized as follows: A bottom metal layer (*the first metal layer*), comprising 2-nm-thick Cr layer and a 15-nm-thick Au layer, was uniformly deposited through electron beam evaporation at a deposition rate of 0.1 $Å s^{-1}$ (Solution PLC-S7, CHA Industries Inc.). A thin film of PNIPAM co-polymerized with acrylic acid (PNIPAM-co-AAC) microgels layer was subsequently "*paint-on*" the bottom metal layer using a fine-tip flat eyeliner brush (Definer Plat N24, Douglas). While it offers sufficient consistency for proof-of-concept evaluation, future implementations aimed at large-scale production or clinical translation would benefit from reagent dispensing systems to ensure reproducibility and precise spatial control. The PNIPAM-co-AAc microgels were synthesized as previously described (Gao et al., 2014). The membranes coated with the PNIPAM-co-AAc microgel layer were dried for 30 min on a hot plate at 35 °C to increase the adhesion between the microgel and the bottom layers. After the drying step, the sample was immersed in Milli-Q® water overnight at 30 °C to remove (*wash off*) the unattached microgels to form a *monolithic microgel* layer. After thoroughly rinsing and drying under N_2 airflow, a top metal layer (*the second metal layer*) identical in composition to the bottom layer was deposited, finalizing the etalon structure. This procedure is schematically described in Fig. 6a. Note that the etalon requires further *functionalization* to become responsive to the target analyte.

2.1.3. Characterization of sensing module in response to temperature

Temperature was chosen as the sensing target for the sensing module. The etalon@membrane was immersed in MQ water (Milli-Q® IQ 7000) and heated on a hot plate (Stuart UC152D, Cole-Parmer™). The corresponding reflectance profiles while increasing the temperature from 20 to 45 °C at 5 °C intervals were recorded using a spectrometer (Ocean Insight FLAME Miniature Spectrometer, Ocean Optics CO, LTD). The spectrometer was coupled with an optical VIS probe (Ocean Insight, Ocean Optics CO, LTD) connected to a light source (Ocean Insight HL-2000-FHSA, Ocean Optics CO, LTD). The reflectance probe tip was positioned 1 mm above the etalon. Reflectance intensity counts were collected using the OceanView 2.0 Ink software at a wavelength range of 400–1000 nm. The width of the boxcar (a built-in smoothing technique that averages a group of adjacent detector elements across spectral data) was set to 25. The scans to average were set to 2, while the remaining settings were left as default. As the light intensity could not be precisely controlled due to model constraints, the intensity counts were normalized to the maximum peak for each profile to compare the peak shift.

2.1.4. Morphology investigation

The surface of the membranes and the etalon@membrane were examined via a scanning electron microscope (SEM, Hitachi Regulus 8230, ST Instruments) to assess both the membranes' morphology and the etalon coating to confirm the formation of a monolithic layer. The membranes were observed after the bottom metal layer was deposited as described previously.

The membrane roughness was analyzed using white light interferometry (Profilm3D, Filmetrics®) with a scanning area of 100 μm × 100 μm, an objective of 50X (Nikon 50x DI), and 10 scan repetitions. The roughness (Sa) and areal material ratio (Smr) were acquired using the ProfilmOnline platform using post-processing functions *Flatten* and *Remove Outliers*.

2.2. Membrane exploration for solution transport

2.2.1. Wicking speed test

The wicking speed of the nylon membrane and RC membrane was assessed before and after coating with an etalon. Water was used as an example solution due to its common use and representative behavior in LFAs. The membranes and etalon@membrane were cut into identical sizes of 5 × 20 mm. Samples were clamped in a bulldog clip and hung above a beaker containing the wicking liquid (Milli-Q® water). With their shorter edge, the samples were then inserted into the Milli-Q® water to initiate the wicking process. The entire process was recorded with an iPhone 14 camera. The height of the propagating liquid front was analyzed in ImageJ (Anon, 2024) and plotted over time t. The experiment was conducted in triplicate. Wicking was performed at constant room conditions of 55% relative humidity and 20 °C.

2.2.2. Permeability test

The permeability of the TE-PC, nylon, and RC membrane was assessed before and after coating with an etalon using milli-Q® water. Each sample was cut into 1 × 1 cm^2 and placed inside a custom-built membrane module as described in our previous work (Kontaxi et al., 2024). The set-up consists of one inlet connected to the milli-Q® water container and one outlet to a collection beaker. The water was pressurized using air and the pressure was controlled via a pressure

controller (Elveflow, OB1 MK3+). The corresponding water flow rate was measured simultaneously using a mass flow meter (mini Coriflow™, Bronkhorst). The membranes' permeability was assessed by measuring the flow rate of permeating water through the membrane under increasing air pressure from 0 mbar to 1000 mbar at intervals of 100 mbar. The test was performed at a constant temperature of 20 °C.

2.3. Demonstration

2.3.1. Glucose etalon sensor fabrication

The separation-sensing function of our EtLFA was demonstrated by filtering a mimic blood solution and sensing the corresponding glucose level. In this demonstration, etalon@Nylon was chosen as the sensing module due to its high sensitivity. The RC membrane was chosen as the separation membrane due to its rapid wicking capability. The configuration of this demonstration is consistent with the general setup shown in the schematic in Fig. 1, where different membranes, including the RC membrane, are used in various experimental configurations.

The PNIPAAm-co-AAC microgel in the etalon was modified specifically to sense glucose. This was achieved by coupling 3-aminophenyl boronic acid monohydrate (APBA) with the carboxyl groups of the acrylic acid. This process is termed as *Carbodiimide-mediated coupling*. The reaction mechanism is schematically illustrated in Fig. 6b. In the presence of glucose, the diols of glucose form covalent bonds with the boronic acid groups (-$B(OH)_2$) of APBA, forming *Boronate–diol complexation* (Badhulika et al., 2014). The formation of boronate complexes increases the negative charge, inducing electrostatic repulsion and causing the microgel to swell.

The APBA modification of microgels is described elsewhere (Sorrell and Serpe, 2012) and is summarized as follows: Etalons@Nylon were immersed in BupH™ 2-(N-morpholino) ethanesulfonic acid Buffered Saline (MES, pH 4.7, Fisher Scientific™). 9 mg of APBA (98%, Sigma-Aldrich) was then added to the buffer solution. The solution and pre-etalon were mixed for 1 h. Following this, 20 mg of 1-ethyl-3-(3-dimethylaminopropyl) carbodiimide (EDC, Thermo Scientific) was added to this solution. The mixture was stirred until complete dissolution. An additional 4.5 mg of APBA was then added to the solution and mixed on the stirrer plate for 30 min. Afterward, a second portion of 20 mg of EDC was added, and once the EDC dissolved, the solution was stored in the refrigerator overnight. The amounts mentioned above were based on a 9 mm^2 sample. The quantities were scaled up proportionally when processing a larger sample.

2.3.2. Glucose-responsive EtLFA assembly

To assemble a glucose-responsive EtLFA, the glucose etalon@Nylon and the RC membrane were cut to the dimensions of 3 × 5 mm^2 and 3 × 10 mm^2, respectively. The processed glucose etalon@Nylon was first mounted onto an adhesive backing (3M 468MP double-sided transfer sheet). The RC membrane was then overlaid onto the glucose etalon@Nylon with a 2 mm overlap in length to complete the assembly of the lateral flow strip. The strip was freshly assembled prior to testing. The assembly steps are schematically described in Fig. 6a.

2.3.3. Mimic blood preparation

The mimic red blood cells were prepared using membrane emulsification of a vortexed mixture containing polydimethylsiloxane (PDMS) and 4% sodium dodecyl sulfate (SDS) to generate PDMS microparticles, representing these cells. The method is described in detail elsewhere (Carneiro et al., 2021) and is summarized below.

The PDMS mixture was prepared by mixing the base with the curing agent (Sylgard®170, Silicone Elastomer Kit, Dow Corning, prepared with a 6:4 ratio of base to curing agent), and 0.1 wt% silicone dye (Fluor Blue, S10151, Siliconesandmore) for better visualization of the PDMS microparticles. The PDMS mixture (oil phase) was then combined with the 4wt% SDS solution (aqueous phase) in a ratio of 4.54:15.46 in a 50 mL centrifugation tube (Corning®, CLS430829). The mixture was vigorously stirred using a vortex mixer (IKA, Vortex 2) at 2500 rpm for 10 min at room temperature. Following emulsification, the mixture underwent additional filtration through 10 μm pore size nylon syringe filters (Tisch Scientific, 25 mm, Luer-Lock/Luer Slip, Nonsterile) to achieve a more controlled emulsion size distribution. Following membrane emulsification, the emulsion was transferred into a glass crystallizing dish and cured at 80 °C for 2 h.

The PDMS microparticles were dried in an oven at a temperature of 35 °C overnight and resuspended in a pH 9.3 carbonate buffer that contains various glucose concentrations to obtain the mimic blood sample. The carbonate buffer was prepared by dissolving 0.38 g of $NaHCO_3$ and 0.055 g of Na_2CO_3 in 1 L of milli-Q® water. Glucose and buffer chemicals are all purchased from Sigma Aldrich®and used as received.

3. Results and discussion

3.1. Membranes exploration of the sensing module

3.1.1. SEM images of membranes and etalon@membranes

To develop the sensing module of the EtLFA, we explored a variety of commercially available membranes to identify the most suitable ones for integration with the PNIPAM-based etalon sensors. Instead of developing new membrane materials, we employ commercially available separation membranes that are already capable of removing components such as red blood cells without the need for off-chip processing. This design choice reflects our goal to leverage, rather than replace, the inherent and well-established separation capabilities of these materials, allowing us to focus on integrating a quantitative optical sensing function. The membranes chosen for this study include track-etched polycarbonate (TE-PC), nylon, regenerated cellulose (RC), polyethersulfone (PES) nitrocellulose (NC), and glass fiber (GF) membranes. These membranes were selected based on their widespread use in existing diagnostic applications (Ahmadi et al., 2015; Li et al., 2017; Muluneh et al., 2014), their diverse material properties, and their potential compatibility with PNIPAM microgel coatings (Kajornprai et al., 2023; Li et al., 2019; Wen and Pelton, 2012).

SEM images of the membranes before (left) and after coating with a gold/PNIPAM/gold etalon structure (right), illustrating the surface characteristics, are shown in Fig. 2. From top to bottom, the pore size of the membranes gradually increases. TE-PC, nylon, RC, and PES membranes show larger planar areas for supporting the microgel beads. In contrast, NC and GF membranes have fibrous and porous structures without planar parts to support the microgel beads. After coating, a uniform layer was observed on the surfaces of TE-PC, nylon, and RC, indicating good adhesion and coverage, with many pores covered with the monolithic microgel layer. The NC membrane resembles a coral-like structure with a porous and irregular surface. The GF membrane is composed of an interconnected network of fibers. These structures provide a high surface area but lack of planar regions for uniform etalon coating. After coating, NC and GF membranes retain their irregularity and rough texture. Despite this, the inset shows that microgels are regularly arranged on the surface of the fibers. This demonstrates that PNIPAM microgel exhibits a strong affinity for these membranes and can be easily coated.

PNIPAM microgel's affinity for our selected membrane materials could be primarily attributed to its hydrophilic nature at temperatures below its lower critical solution temperature. Especially, PNIPAM contains a large number of amide groups that are capable of both donating and accepting hydrogen bonds (Schild, 1992). The nitrogen and oxygen in these amide groups can form hydrogen bonds with other polar groups in the membranes. The hydrophilicity allows PNIPAM to easily interact with polar functional groups of membrane materials, such as the sulfone and ether groups in the PES, the nitro groups in the NC, the amide groups in the nylon, the silanol groups in the GF. The ability of PNIPAM to form hydrogen bonds further boosts its compatibility with diverse membrane types that have been demonstrated in detail elsewhere (Liu et al., 2017; Zhu et al., 2019; Kajornprai et al., 2023; Li et al., 2019; Wen and Pelton, 2012; Ormategui et al., 2012).

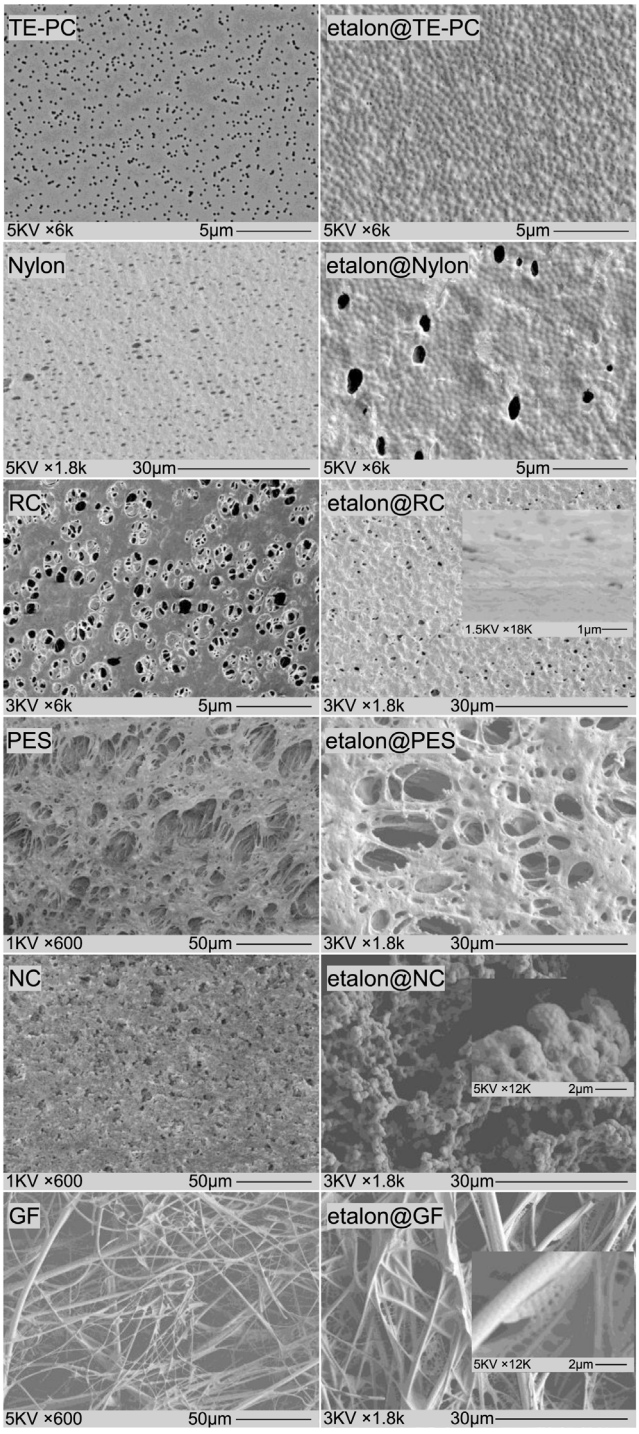

Fig. 2. SEM images of the commercial membranes before (left) and after (right) etalon integration. The membranes, from top to bottom, are track-etched PC (TE-PC), nylon, regenerated cellulose (RC), polyethersulfone (PES), nitrocellulose (NC), and glass fiber (GF) membranes respectively. Insets show magnified views: etalon@RC at 18k magnification, etalon@NC at 12k magnification, and etalon@GF at 12k magnification.

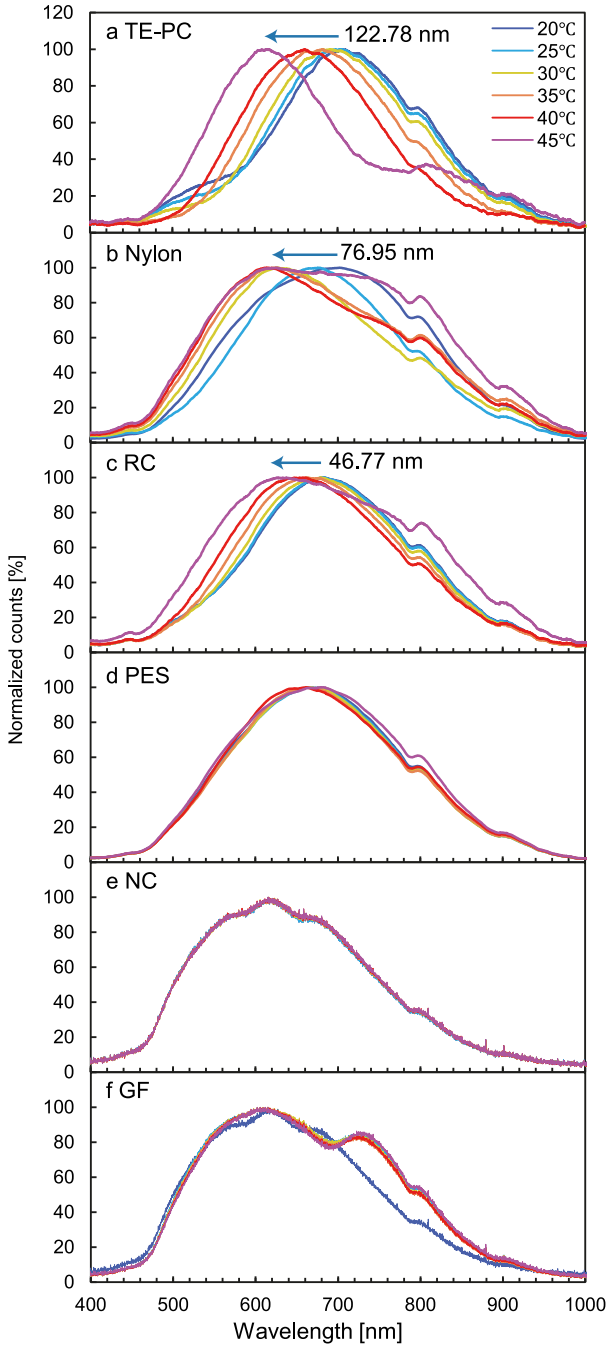

Fig. 3. Reflectance profiles of etalon integrated on different membranes at various temperatures. The membranes are: (a) track-etched polycarbonate (ET-PC), (b) nylon, (c) regenerated cellulose (RC), (d) polyethersulfone (PES), (e) nitrocellulose (NC), and (f) glass fiber (GF) membrane.

3.1.2. Sensitivity of etalon@membranes

The reflection spectra of all the etalon@membranes are illustrated in Fig. 3. All the etalon@membrane show only one significant peak at around 600 to 700 nm. As the temperature rises from 20 °C to 45 °C, the PNIPAM microgel gradually collapses, causing the gold mirrors to approach to each other. With increasing the temperature as the stimulus, an etalon is expected to display a spectral blue shift (a shift from longer to shorter wavelengths). Figs. 3a–3c show that the etalons coated on TE-PC, nylon, and RC experienced blue shifts of approximately 122.78 nm, 76.95 nm, and 46.77 nm, respectively. In contrast, etalons coated on PES, NC, and GF (Figs. 3d–3f) did not exhibit a noticeable peak shift. The maximum peak shifts, taken as the sensitivity of each etalon, were respectively, 122.78 nm, 76.95 nm, 46.77 nm, 3.11 nm, 0 nm, and 0 nm from top to bottom. These findings suggest that etalons fabricated on membranes with larger supporting areas and lower surface roughness tend to exhibit higher sensitivity.

It is worth noting that while LFAs are typically used for detecting specific bioanalytical targets, temperature serves as a convenient

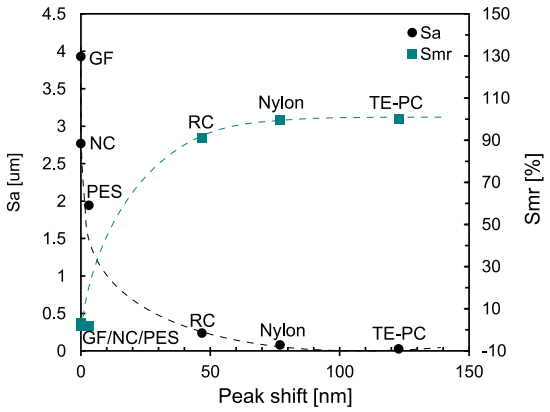

Fig. 4. The correlation between membrane surface roughness and etalon sensitivity. The dashed lines are guides for the eye.

and well-controlled model parameter to evaluate the performance and sensitivity of the etalon@membranes. Using temperature allows us to assess the etalon's performance based on solely the membrane properties, eliminating the need to consider interactions between biological analytes and the membrane and/or etalon.

3.1.3. Correlation between roughness and etalon sensitivity

The correlation between surface topography of membranes and etalon sensitivity is further examined in Fig. 4. The membranes' surface topography is characterized by average roughness(Sa) and areal material ratio (Smr) respectively. Sa represents the arithmetic mean height of the surface, giving the average of absolute height values across the entire surface, while Smr indicates the percentage of the surface that lies above a specified height level (Filmetrics.com, 2020).

As illustrated in Fig. 4, etalons fabricated on membranes with low Sa and high Smr, namely TE-PC, nylon, and RC membranes, demonstrate enhanced sensitivity. A large areal material ratio indicates a larger solid surface available to support microgels. Meanwhile, low Sa suggests a smoother and flatter substrate surface, facilitating the formation of a uniform microgel layer with minimal gaps or height variations. This monolithic microgel layer ensures consistent parallel passage of light through each bead, thereby preventing destructive interference. These results show that the membrane surface roughness criteria to achieve a successful etalon sensor are (a) Sa value below 0.5 μm, and (b) Smr value above 90%.

The results of this study confirm that integrating etalon sensors onto commercial membranes is feasible. Our findings indicate that membrane surface roughness plays a critical role in determining sensor sensitivity, with smoother membranes yielding higher sensitivity. Consequently, TE-PC, nylon, and RC membranes emerge as prime candidates for our integrated separation-sensing microfluidic platforms.

3.2. Membrane exploration for solution transport: assessing wicking and permeability properties

3.2.1. Wicking speed

An essential property of membranes for LFAs is their capillary force, which determines the solution transport efficiency. Fig. 5a compares the water wicking speeds of nylon (teal squares) and RC membranes (black circles) before (solid symbols) and after etalon integration (open symbols). For nylon, etalon coating slightly increases the wicking speed, whereas for RC membranes, it significantly enhances it.

This enhancement may result from (1) the hydrophilic nature of PNIPAM aiding water absorption, (2) PNIPAM-induced pore transformations reducing internal pore pressure and increasing capillary forces (Kalish et al., 2020), as corroborated by SEM images in Fig. 2, and (3) reduced effective membrane pore size due to PNIPAM coating (Kontaxi et al., 2024).

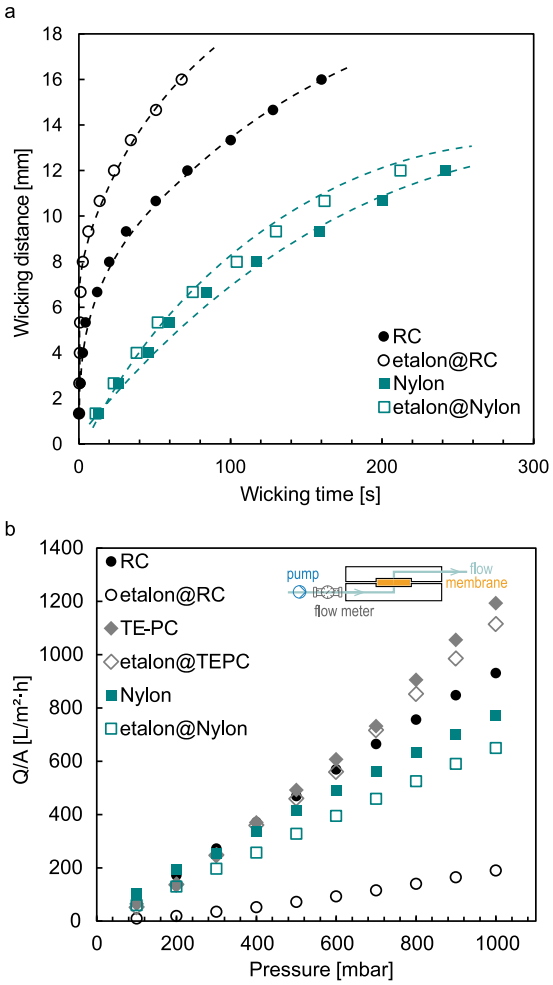

Fig. 5. (a) Wicking speed test on regenerated cellulose membranes (black) and nylon membrane (teal) before (solid symbols) and after (open symbols) etalon integration. The dashed lines are guides for the eye. (b) Comparison of the permeating water flux through the RC (black), TE-PC (gray), and nylon (teal) membranes before (solid symbols) and after (open symbols) etalon integration as a function of pressure. The inset presents a schematic diagram of the experimental setup designed for assessing membrane permeability.

These findings indicate that etalon coatings can boost wicking efficiency without compromising it due to potential pore narrowing. By controlling the coverage area of the etalon on the membrane surface, the wicking capability can be further modulated. This introduces the opportunity to design and include transport channels with specific configurations/dimensions on the LFAs.

3.2.2. Permeability and permeance

Permeability experiments were conducted to evaluate the membrane performance before and after etalon integration. Fig. 5b illustrates the water flux permeability as a function of applied pressure. A significant reduction in permeating flux is observed in membranes after etalon integration. This is mainly due to the uniform coverage of the microgel layer across the membrane surface, as evidenced by the SEM images (Fig. 2). This coverage modifies the surface structure, effectively sealing most pores and reducing permeability. Additionally, the increased thickness due to the etalon layer likely contributes to higher resistance, further limiting water flow through the membrane. These combined effects underline the impact of the integration process on the membrane's functionality.

Table 1
Pore radius reduction, microgel layer thickness (δ), and percentage of pore radius reduction at P_{max} = 1 bar at 25°C.

Membrane	r_p (μm)	r_{et} (μm)	δ (μm)	Reduction
RC	0.10	0.071	0.029	29.2%
TE-PC	0.10	0.098	0.0017	1.7%
Nylon	0.10	0.095	0.045	4.5%

Table 2
Permeance of the membranes before and after etalon integration, along with the percentage reduction in permeance. Permeance values are derived as the slope of the flux vs. pressure plot (Fig. 5b).

Membrane	Permeance (L/m^2 h bar)		Reduction
	Before	After	
RC	907.2 ± 71.2	145.3 ± 34.3	84.0%
TE-PC	950.1 ± 217.1	920.4 ± 164.0	3.2%
Nylon	850.5 ± 90.9	648.1 ± 17.5	23.8%

The extent of flux reduction becomes more pronounced at higher pressures. For instance, at 1000 mbar, the RC membrane's flux decreases 79.6% (from 931 L/m^2 h to 190 L/m^2 h) after microgel coating, while at 200 mbar, the reduction is 88.7% (from 172 L/m^2 h to 19.4 L/m^2 h). These observations suggest two key insights. First, pressure amplifies the microgel response in its swollen state. This is expected as water absorption increases microgel elasticity, causing pore narrowing (Kontaxi et al., 2024) and reduced flow rates. Second, the near-linear pressure–flux relationship observed across membranes indicates that the pores remain open, with TE-PC showing minimal flux reduction even in the swollen state.

The permeating flux values through the membranes at high pressures, together with pore wall coverage by microgel beads, are used to define the "effective pore radius" (r_{et}). The calculation of r_{et} is based on the Hagen–Poiseuille law (Eq. (1)):

$$Q = \frac{\pi r^4 \Delta P}{8 \mu L} \tag{1}$$

where μ (Pa s) represents the dynamic viscosity, Q (m^3 s^{-1}) denotes the volumetric flow rate, and $\Delta P/L$ (Pa m^{-1}) indicates the pressure gradient across the membrane.

Assuming equivalent pressure gradients for both the pristine and etalon membranes, the effective pore radius corresponding to each pressure gradient is calculated using Eq. (2) (Kontaxi et al., 2024):

$$r_{et} = r_p \left(\frac{Q_{et}}{Q_p} \right)^{1/4} \tag{2}$$

where r_{et} is the effective pore radii of the etalon@membranes, r_p (m) is the pore radii before coating, Q_{et} and Q_p (m^3 s^{-1}) are the flow rates through the microgel-coated etalon and non-coated membranes, respectively.

The reduction in the effective pore radius, defined as the difference between r_{et} and the pristine pore radius, and thickness of the microgel layer that coats the pore wall (δ) provide valuable insights into the impact of the microgel layer on membrane permeability. This information is summarized in Table 1. δ is determined by subtracting the etalon pore radius (determined using Eq. (2)) from the pristine pore radius (0.10 μm) at maximum pressure (1 bar).

Using the data from Fig. 5b, the pressure-normalized flux, or permeance, was calculated and summarized in Table 2. Permeance is a useful metric, particularly for composite membranes with unknown or variable thickness, and is defined in Eq. (3) (Kontaxi et al., 2024):

$$P_e = \frac{Q/A}{\Delta P} \tag{3}$$

where Q/A (L/m^2 h) is the flux, ΔP (bar) is the pressure difference, and P_e (L/m^2 h bar) represents the pressure-normalized flux (permeance).

For nylon and RC membranes, the permeance decreases significantly by 84.0% and 23.8%, respectively, after coating. TE-PC on the other hand exhibits a negligible decrease (3.2%) in permeance, potentially due to its distinct pore structure. Unlike the irregular pores of nylon or RC, TE-PC features track-etched tubular pores are through holes, providing lower resistance to water flow. These tubular pores prevent pore blockage, maintaining high permeability even in conditions prone to severe fouling or particulate buildup. High wicking speed and low permeability in membranes, like nylon and RC, are advantageous for applications requiring controlled fluid transport, such as lateral flow assays and liquid distribution in diagnostics. These characteristics ensure efficient liquid spreading while minimizing excessive flow. On the other hand, membranes with high permeability, such as TE-PC, are ideal for sensors, including sweat and biosensors, where rapid fluid transport is crucial for real-time monitoring and accurate detection. These properties enable tailored solutions for both analytical and wearable sensor applications (Moonen et al., 2023).

3.3. Demonstration device

Fig. 6c and d shows a real instance of our device, a glucose-responsive EtLFA, which consists a RC separation module and an etalon@nylon membrane sensing module. When a mimic blood solution is applied, blue particles, mimicking red blood cells, are effectively retained at the RC membrane (blue dots as indicated by the black arrows and circled in red in Fig. 6d), while the liquid wicks to the sensing area. Upon exposure to 100 mg/dL glucose, the sensing area undergoes a visible color shift from magenta to light blue (highlighted in yellow in Fig. 6d), providing a binary detection signal.

Glucose was selected as a model analyte due to the ease of reagent preparation, availability, and compatibility with PNIPAM-based etalon systems. This choice allowed us to validate the quantitative optical behavior of the etalon layer under capillary flow in a controlled manner. The use of glucose, rather than specific bioreceptors like antibodies, was motivated by our study's core goal: to demonstrate the feasibility of integrating etalon structures onto commercial membranes while maintaining optical functionality. We therefore did not introduce additional complexity through biofunctionalization, which has been widely addressed in previous studies.

To better evaluate the EtLFA system's performance, we compared it with other glucose detection techniques. The most common method in clinical settings is the use of commercial glucose meters, which offer fast and accurate measurements but are limited to serum samples and not suitable for whole-blood LFA integration (Villena Gonzales et al., 2019). Paper-based colorimetric methods have also been developed for glucose detection using glucose oxidase (GOD) as a recognition element (Van Tam et al., 2021; Huang et al., 2022). While such platforms are inexpensive and easy to operate, they typically suffer from poor quantification capability, background interference, and a lack of compatibility with lateral flow formats. In particular, these systems are not typically integrated into LFA-style strips and often require manual sample handling and reagent mixing. Moreover, conventional LFAs are generally designed for macromolecule detection, such as proteins, using sandwich-type immunoassays. However, detecting small molecules like glucose is inherently challenging in this format because they lack suitable antibody pairs and do not form sandwich complexes. As a result, glucose detection in LFA devices remains limited and often lacks quantification capability.

In contrast, our EtLFA employs a fundamentally different sensing mechanism based on optical interference. The glucose-responsive hydrogel's volumetric changes induce a wavelength shift in the reflectance spectrum, enabling robust, ratiometric detection less affected by intensity fluctuations or background light. This approach allows for accurate and portable quantification, will be shown by the linear calibration curve in Fig. 6e.

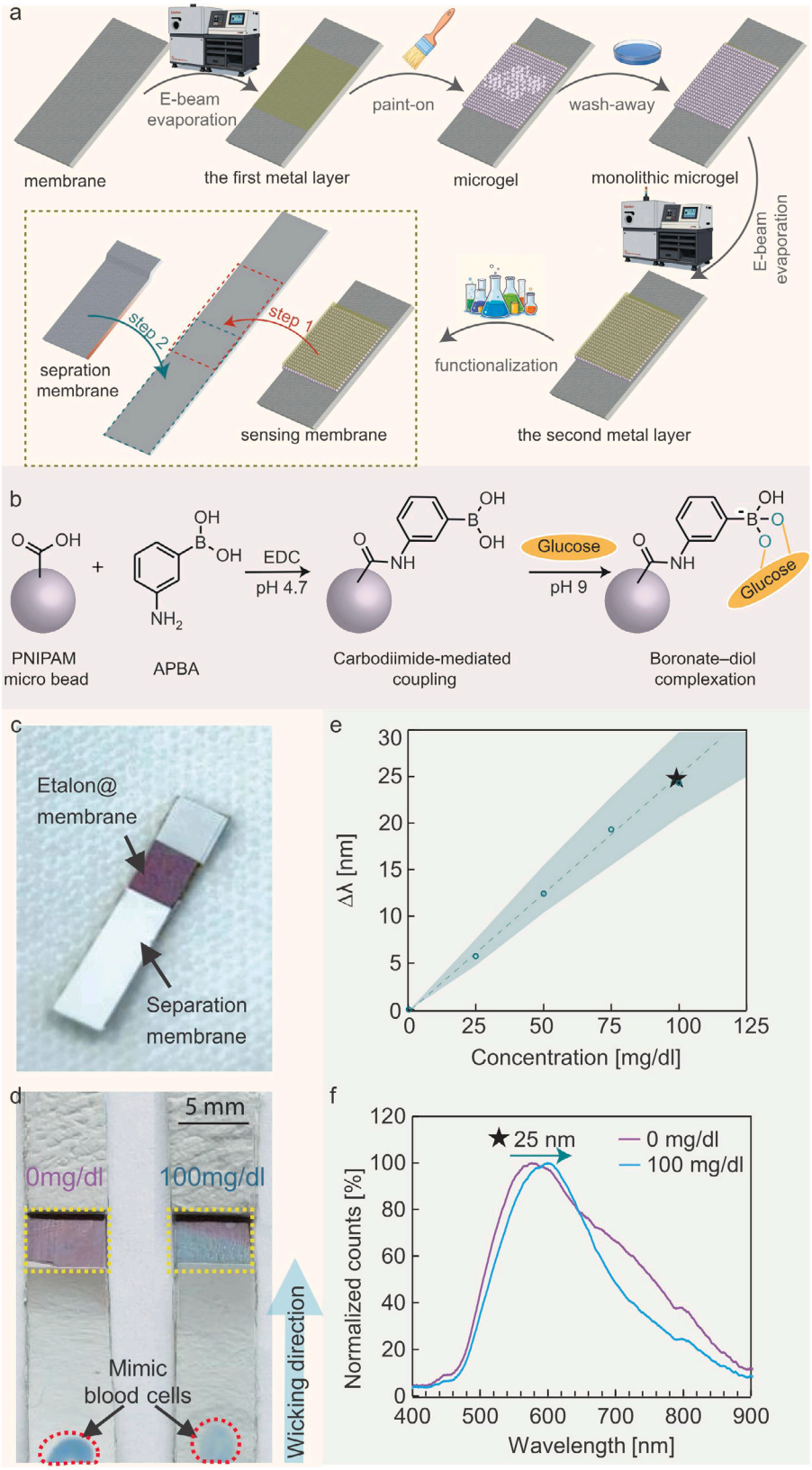

Fig. 6. (a) The schematic representation of the EtLFA fabrication process. (b) Reaction scheme illustrating the functionalization of acrylic acid groups on the microgel using 3-aminophenylboronic acid (APBA), followed by base-induced activation of the boronic acid. The –OH group highlighted in teal binds to glucose upon its presence. (c) A real instance of the EtLFA. (d) A glucose-responsive EtLFA. The EtLFA efficiently retains all mimic blood cells (circled in red) at the bottom of the strip. Upon exposure to glucose, the sensing area (highlighted in yellow) exhibits a visible color change from magenta to light blue. The wicking direction proceeds from bottom to top. (e) Calibration curve correlating glucose concentration to the observed spectral peak shift ($\Delta\lambda$). The teal dashed line with circular markers represents the mean shift, and the shaded region indicates the standard deviation across three replicates. (f)Reflectance spectra of the EtLFA device at glucose concentrations of 0 and 100 mg/dL. A peak shift of 25 nm is observed.

Fig. 6e and f highlight the quantitative capability of the EtLFA device. The glucose detection mechanism is based on the shift in the reflectance spectrum ($\Delta\lambda$). Fig. 6e represents the calibration curve that maps glucose concentration to the observed shift. The dashed teal line with circular markers illustrates the linear relationship between $\Delta\lambda$ and glucose concentration. The shaded region represents the standard deviation across three replicates, confirming the device's precision and reliability. Fig. 6f corresponds to the reflectance spectrum at glucose concentrations of 0 and 100 mg/dL. A peak shift of 25 nm (from 580 nm to 605 nm) is observed. Based on the calibration curve, this shift corresponds to a glucose concentration of 100 mg/dL (indicated by a star), consistent with the pre-prepared sample.

By this glucose-responsive EtLFA, we demonstrate that our EtLFA can perform sample purification by effectively retaining mimic red blood cells. It provides a binary Yes/No answer through quick and straightforward identification of analytes via a noticeable colorimetric reaction. It can further provide a quantitative measurement of the analyte concentration when combined with a portable reflectance spectrometer. These characteristics make our device practical and effective for on-the-spot testing situations.

In clinical practice, accurate blood–glucose measurement remains challenging due to numerous endogenous interferents. Lipids such as cholesterol can alter membrane wettability and capillary flow (Raffy and Teissié, 1999), while elevated lactate — produced during exercise or infection — can compete with glucose for boronate binding. Serum albumin may form complexes with sugars or nonspecifically adsorb to sensing components, and aberrant albumin levels are themselves a marker of metabolic dysfunction. Likewise, renal impairment in diabetic patients can raise blood urea concentrations, shifting refractive-index baselines and leading to erroneous glucose readings. Therefore, we selected mimic blood rather than real blood to eliminate unpredictable biological interferences, while preserving key physical properties. The mimic solution contains a surfactant to simulate plasma-like fluid behavior and PDMS microspheres to represent red blood cells, enabling a clear and controlled demonstration of the separation–detection mechanism. In contrast, real blood samples contain a complex mixture of components that can affect detection accuracy—for example, APBA may bind not only to glucose but also to other cis-diol sugars such as fructose or glycoprotein carbohydrates, causing cross-reactivity (Di Pasquale, 2022). Additionally, endogenous substances like ascorbic acid or uric acid could non-specifically interact with boronic acid groups or alter the refractive index, resulting in false spectral shifts (Li and Liu, 2015). Physiological factors including blood viscosity, pH, and ionic strength further influence capillary flow and the equilibrium of the APBA–glucose complex. These challenges highlight the importance of optimizing assay conditions, such as pH and ionic strength, to improve selectivity and accuracy when working with real blood. Our current use of a regenerated cellulose membrane helps mitigate some interferences by rapidly wicking away large proteins and cellular debris (Park et al., 2025). However, future studies employing real blood will require thorough testing of selectivity against common interferents, evaluation of reproducibility, spike-and-recovery experiments, and stability assessments to fully validate device performance under clinically relevant conditions.

This demonstration serves as a proof-of-concept to showcase the feasibility of integrating etalon structures onto unmodified commercial membranes for quantitative detection under capillary flow. As such, the system was validated using a model analyte and synthetic blood mimic, rather than optimized for full analytical performance. Future research should systematically investigate several critical analytical parameters to advance this platform toward practical applications. These include determining the limit of detection (LOD), limit of quantification (LOQ), dynamic range, and signal reproducibility. Additionally, selectivity studies in the presence of physiologically relevant interferents such as lactate, uric acid, and glycoproteins will be essential to validate real-world performance. Such efforts will be key to transforming this platform into a reliable diagnostic tool for clinical, environmental, or forensic use.

To ensure reliable performance in real-world applications, the factors that may influence the long-term stability of the device should also be considered. These include membrane degradation due to repeated wet–dry cycles, which can affect capillary flow; fatigue of the PNIPAAm-co-AAC microgel network under prolonged physiological exposure; potential delamination or oxidation of the Cr/Au thin films on the rough substrate; and fouling from sample residues, which may cause baseline drift in the reflectance signal. Addressing these potential issues through material optimization and system-level engineering will be critical for future development and clinical translation of the platform.

4. Conclusion

This study introduces a novel strategy for integrating separation and sensing functionalities into a single microfluidic platform using etalon-modified lateral flow strips. By combining surface roughness analysis, wicking, and permeance measurements, we provide insights into the relationship between membrane properties and the etalon's optical and fluidic performance. A practical criteria for selecting membranes for etalon production is further established. The successful demonstration of the glucose-responsive EtLFA showcases its dual functionality: effective sample purification by retaining mimic red blood cells and analyte detection through a visible color change upon exposure to glucose. The device highlights the potential of our design to offer enhanced analytical capabilities and broaden the applications of lateral flow assays. Future work will focus on improving membrane functionalization and expanding analyte specificity to fully realize the quantitative potential of this platform in clinical and environmental settings. Further exploration, particularly in chemical modification of PNIPAM and membrane optimization, holds promise for advancing quantitative testing of various analytes, thereby contributing to advancements in real-time health diagnostics, environmental contaminant monitoring, and forensic analyte detection.

CRediT authorship contribution statement

Mengmeng Zhang: Writing – original draft, Visualization, Methodology, Investigation. **Arjo J. Loeve:** Writing – review & editing, Supervision, Resources, Methodology, Funding acquisition, Conceptualization. **Michael J. Serpe:** Writing – review & editing, Methodology. **Hanieh Bazyar:** Writing – review & editing, Supervision, Resources, Methodology, Funding acquisition, Conceptualization.

Declaration of competing interest

The authors declare that they have no known competing financial interests or personal relationships that could have appeared to influence the work reported in this paper.

Acknowledgments

H. Bazyar and A. J. Loeve wish to acknowledge faculty of Mechanical Engineering, Delft University of Technology, Netherlands, for funding this project as part of the cohesion grants.

Data availability

Data will be made available on request.

References

Ahmadi, Housna Shamloo, Heiat, Mohammad, Rashedi, Hamid, Latifi, Ali Mohammad, 2015. Utilizing different supports and comparing their performances in the construction of morphine rapid detection system based on lateral flow assay. J. Appl. Biotechnol. Rep. 2 (1), 199–202.

Anon, 2024. Features — imagej.net. https://imagej.net/ij/features.html. (Accessed 10 October 2024).

Badhulika, Sushmee, Tlili, Chaker, Mulchandani, Ashok, 2014. Poly (3-aminophenylboronic acid)-functionalized carbon nanotubes-based chemiresistive sensors for detection of sugars. Analyst 139 (12), 3077–3082.

Budd, Jobie, Miller, Benjamin S., Weckman, Nicole E., Cherkaoui, Dounia, Huang, Da, Decruz, Alyssa Thomas, Fongwen, Noah, Han, Gyeo-Re, Broto, Marta, Estcourt, Claudia S., Gibbs, Jo, Pillay, Deenan, Sonnenberg, Pam, Meurant, Robyn, Thomas, Michael R., Keegan, Neil, Stevens, Molly M., Nastouli, Eleni, Topol, Eric J., Johnson, Anne M., Shahmanesh, Maryam, Ozcan, Aydogan, Collins, James J., Fernandez Suarez, Marta, Rodriguez, Bill, Peeling, Rosanna W., McKendry, Rachel A., 2023. Lateral flow test engineering and lessons learned from COVID-19. Nat. Rev. Bioeng. 1, 13–31.

Cao, Yuanyuan, Wang, Yapei, 2016. Temperature-mediated regulation of enzymatic activity. ChemCatChem 8 (17), 2740–2747.

Carneiro, J., Lima, R., Campos, JB.L.M., Miranda, J.M., 2021. A microparticle blood analogue suspension matching blood rheology. Soft Matter 17 (14), 3963–3974.

Chen, Guohua, Hoffman, Allan S., 1994. Synthesis of carboxylated poly (NIPAAm) oligomers and their application to form thermo-reversible polymer-enzyme conjugates. J. Biomater. Sci. Polym. Ed. 5 (4), 371–382.

Das, Anubhab, Babu, Anashwara, Chakraborty, Sourav, Van Guyse, Joachim FR, Hoogenboom, Richard, Maji, Samarendra, 2024. Poly (N-isopropylacrylamide) and its copolymers: a review on recent advances in the areas of sensing and biosensing. Adv. Funct. Mater. 34 (37), 2402432.

Davies, C., 2013. Principles of competitive and immunometric assays (Including ELISA). In: Wild, D. (Ed.), The Immunoassay Handbook, fourth ed. Elsevier, pp. 29–59.

Dey, Mohan Kumar, Iftesum, Maria, Devireddy, Ram, Gartia, Manas Ranjan, 2023. New technologies and reagents in lateral flow assay (LFA) designs for enhancing accuracy and sensitivity. Anal. Methods 15 (35), 4351–4376.

Di Pasquale, Alice, 2022. Design and synthesis of multivalent receptors towards the detection of biologically relevant carbohydrates (Ph.D. thesis). University of Birmingham.

Du, Xiaoxue, He, Ping-Ping, Wang, Chunyan, Wang, Xiaowen, Mu, Yali, Guo, Weiwei, 2023. Fast transport and transformation of biomacromolecular substances via thermo-stimulated active ‘‘inhalation–exhalation’’ cycles of hierarchically structured smart pNIPAM–DNA hydrogels. Adv. Mater. 35 (2), 2206302.

Filmetrics.com, 2020. Profilm3D software user manual. https://www.phys.sinica.edu.tw/~bssf/docs/Profilm3D_Software_User_Manual.pdf. (Accessed 10 October 2024).

Fuentes-Chust, Celia, Parolo, Claudio, Rosati, Giulio, Rivas, Lourdes, Perez-Toralla, Karla, Simon, Stéphanie, de Lecuona, Itziar, Junot, Christophe, Trebicka, Jonel, Merkoçi, Arben, 2021. The microbiome meets nanotechnology: opportunities and challenges in developing new diagnostic devices. Adv. Mater. 33 (18), 2006104.

Gao, Yongfeng, Xu, Wenwen, Serpe, Michael J., 2014. Free-standing poly (N-isopropylacrylamide) microgel-based etalons. J. Mater. Chem. C 2 (29), 5878–5884.

Gubala, Vladimir, Harris, Leanne F, Ricco, Antonio J, Tan, Ming X, Williams, David E, 2012. Point of care diagnostics: status and future. Anal. Chem. 84 (2), 487–515.

Gumus, Eda, Bingol, Haluk, Zor, Erhan, 2023. Lateral flow assays for detection of disease biomarkers. J. Pharm. Biomed. Anal. 225, 115206.

Guo, Weiwei, Lu, Chun-Hua, Qi, Xiu-Juan, Orbach, Ron, Fadeev, Michael, Yang, Huang-Hao, Willner, Itamar, 2014. Switchable bifunctional stimuli-triggered poly-N-isopropylacrylamide/DNA hydrogels. Angew. Chem. Int. Ed. 53 (38), 10134–10138.

Herrmann, Anna, Haag, Rainer, Schedler, Uwe, 2021. Hydrogels and their role in biosensing applications. Adv. Heal. Mater. 10 (11), 2100062.

Huang, Hsiao-Jung, Lin, Yu-Ting, Chung, Min-Chi, Chen, Yu-Hsuan, Tan, Kui-Thong, 2022. Glucose and ethanol detection with an affinity-switchable lateral flow assay. Anal. Chem. 94 (12), 5084–5090.

İnce, Bahar, Uludağ, İnci, Demirbakan, Burçak, Özyurt, Canan, Özcan, Burcu, Sezgintürk, Mustafa Kemal, 2023. Lateral flow assays for food analyses: Food contaminants, allergens, toxins, and beyond. TRAC Trends Anal. Chem. 169, 117418.

Jara, Marcia Daniela Lazo, Alvarez, Luis Alberto Contreras, Guimarães, Marco CC, Antunes, Paulo Wagnner Pereira, de Oliveira, Jairo Pinto, 2022. Lateral flow assay applied to pesticides detection: recent trends and progress. Environ. Sci. Pollut. Res. 29 (31), 46487–46508.

Jiang, Yaxin, Colazo, Marcos G., Serpe, Michael J., 2016. Poly (N-isopropylacrylamide) microgel-based sensor for progesterone in aqueous samples. Colloid Polym. Sci. 294 (11), 1733–1741.

Jiang, Yaxin, Colazo, Marcos G., Serpe, Michael J., 2018. Poly (N-isopropylacrylamide) microgel-based etalons for the label-free quantitation of estradiol-17β in aqueous solutions and milk samples. Anal. Bioanal. Chem. 410, 4397–4407.

Kajornprai, Todsapol, Katesripongsa, Putita, Nam, Sang Yong, Hamid, Zuratul Ain Abdul, Ruksakulpiwat, Yupaporn, Suppakarn, Nitinat, Trongsatitkul, Tatiya, 2023. Potential applications of thermoresponsive poly (N-Isoproplacrylamide)-grafted nylon membranes: Effect of grafting yield and architecture on gating performance. Polymers 15 (3), 497.

Kakkar, Saloni, Gupta, Payal, Singh Yadav, Shiv Pratap, Raj, Divakar, Singh, Garima, Chauhan, Sakshi, Mishra, Manoj Kumar, Martín-Ortega, Elena, Chiussi, Stefano, Kant, Krishna, 2024. Lateral flow assays: Progress and evolution of recent trends in point-of-care applications. Mater. Today Bio (ISSN: 2590-0064) 28, 101188.

Kalish, Brent, Tan, Mick Kyle, Tsutsui, Hideaki, 2020. Modifying wicking speeds in paper-based microfluidic devices by laser-etching. Micromachines 11 (8), 773.

Khatmi, Gazy, Klinavičius, Tomas, Simanavičius, Martynas, Silimavičius, Laimis, Tamulevičienė, Asta, Rimkutė, Agnė, Kučinskaitė-Kodzė, Indrė, Gylys, Gintautas, Tamulevičius, Tomas, 2024. Lateral flow assay sensitivity and signal enhancement via laser μ -machined constrains in nitrocellulose membrane. Sci. Rep. 14, 22936.

Koczula, Katarzyna M., Gallotta, Andrea, 2016. Lateral flow assays. Essays Biochem. 60 (1), 111–120.

Kontaxi, G, Wensink, G, Sberna, PM, Rücker, M, Garbin, V, Serpe, MJ, Bazyar, H, 2024. Microgel-based etalon membranes: Characterization and properties. APL Mater. 12 (9).

Lanzalaco, Sonia, Mingot, Júlia, Torras, Juan, Alemán, Carlos, Armelin, Elaine, 2023. Recent advances in poly (N-isopropylacrylamide) hydrogels and derivatives as promising materials for biomedical and engineering emerging applications. Adv. Eng. Mater. 25 (4), 2201303.

Lee, Shih-Hui, Hoshino, Yu, Randall, Arlo, Zeng, Zhiyang, Baldi, Piere, Doong, Ruey-an, Shea, Kenneth J, 2012. Engineered synthetic polymer nanoparticles as IgG affinity ligands. J. Am. Chem. Soc. 134 (38), 15765–15772.

Li, H., Han, D., Hegener, M.A., Pauletti, G.M., Steckl, A.J., 2017. Flow reproducibility of whole blood and other bodily fluids in simplified no reaction lateral flow assay devices. Biomicrofluidics 11 (2), 024116.

Li, Daojin, Liu, Zhen, 2015. Boronate affinity materials for the selective capture of cis-diol-containing biomolecules.

Li, Juan, Mo, Liuting, Lu, Chun-Hua, Fu, Ting, Yang, Huang-Hao, Tan, Weihong, 2016. Functional nucleic acid-based hydrogels for bioanalytical and biomedical applications. Chem. Soc. Rev. 45 (5), 1410–1431.

Li, Xiao-Ying, Xie, Rui, Zhang, Chuan, Chen, Zhi-Hao, Hu, Jia-Qi, Ju, Xiao-Jie, Wang, Wei, Liu, Zhuang, Chu, Liang-Yin, 2019. Effects of hydrophilicity of blended submicrogels on the microstructure and performance of thermo-responsive membranes. J. Membr. Sci. 584, 202–215.

Liu, Jingchong, Wang, Nü, Yu, Li-Juan, Karton, Amir, Li, Wen, Zhang, Weixia, Guo, Fengyun, Hou, Lanlan, Cheng, Qunfeng, Jiang, Lei, et al., 2017. Bioinspired graphene membrane with temperature tunable channels for water gating and molecular separation. Nat. Commun. 8 (1), 2011.

Liu, Min, Yi, Kezhen, Zhang, Yaran, Long, Fei, Hu, Xin, Jia, Gaihua, Xiao, Ting, Xu, Xianqun, Duan, Yongwei, Shi, Hongjie, et al., 2024. Enhanced exosome capture in urine using aptamer-modified temperature-responsive polymer for sensitive early detection of bladder cancer. Chem. Eng. J. 489, 151304.

Maekawa, Yutaro, Ayano, Eri, Nagase, Kenichi, Kanazawa, Hideko, 2021. Effective separation for new therapeutic modalities utilizing temperature-responsive chromatography. Anal. Sci. 37 (5), 651–660.

Mark, Daniel, Haeberle, Stefan, Roth, Günter, Von Stetten, Felix, Zengerle, Roland, 2010. Microfluidic lab-on-a-chip platforms: requirements, characteristics and applications. Microfluid. Based Microsyst.: Fundam. Appl. 305–376.

Moonen, Emma JM, ul Islam, Tanveer, van Kemenade, Sebastiaan, Pelssers, Eduard, Heikenfeld, Jason, den Toonder, Jaap MJ, 2023. A versatile artificial skin platform for sweat sensor development. Lab A Chip 23 (9), 2268–2275.

Muluneh, Melaku, Shang, Wu, Issadore, David, 2014. Track-etched magnetic micropores for immunomagnetic isolation of pathogens. Adv. Heal. Mater. 3 (7), 1078–1085.

Nam, Seunghyeon, Kim, Hyojung, Lee, Sang-Mok, Durukan, Mete Batuhan, Unalan, Husnu Emrah, Lee, Hyunjoo J, 2023. A glucose-responsive microgel-based soft etalon as an epidermal glucose colorimetric sensor. Sensors Actuators B: Chem. 396, 134554.

Ormategui, Nerea, Zhang, Shengwen, Loinaz, Iraida, Brydson, Rik, Nelson, Andrew, Vakurov, Alexander, 2012. Interaction of poly (N-isopropylacrylamide)(pNIPAM) based nanoparticles and their linear polymer precursor with phospholipid membrane models. Bioelectrochemistry 87, 211–219.

Park, Inho, Kang, Jun Hyeok, Ha, Yelim, Lee, Junhyeong, Park, Ho Bum, 2025. Hydrothermally rearranged cellulose membranes for controlled size sieving. J. Membr. Sci. 713, 123367.

Pedreira-Rincón, Julia, Rivas, Lourdes, Comenge, Joan, Skouridou, Vasso, Camprubí-Ferrer, Daniel, Muñoz, Jose, O'Sullivan, Ciara K., Chamorro-Garcia, Alejandro, Parolo, Claudio, 2025. A comprehensive review of competitive lateral flow assays over the past decade. Lab Chip.

Raffy, Sophie, Teissié, Justin, 1999. Control of lipid membrane stability by cholesterol content. Biophys. J. 76 (4), 2072–2080.

Sadeghi, Poorya, Sohrabi, Hessamaddin, Hejazi, Maryam, Jahanban-Esfahlan, Ali, Baradaran, Behzad, Tohidast, Maryam, Majidi, Mir Reza, Mokhtarzadeh, Ahad, Tavangar, Seyed Mohammad, de la Guardia, Miguel, 2021. Lateral flow assays (LFA) as an alternative medical diagnosis method for detection of virus species: The intertwine of nanotechnology with sensing strategies. TRAC Trends Anal. Chem. 145, 116460.

Schild, Howard G., 1992. Poly (N-isopropylacrylamide): experiment, theory and application. Prog. Polym. Sci. 17 (2), 163–249.
Sena-Torralba, Amadeo, Álvarez-Diduk, Ruslan, Parolo, Claudio, Piper, Andrew, Merkoçi, Arben, 2022. Toward next generation lateral flow assays: integration of nanomaterials. Chem. Rev. 122 (18), 14881–14910.
Shaibie, Nur Adania, Ramli, Nurul Afina, Mohammad Faizal, Nur Dini Fatini, Srichana, Teerapol, Mohd Amin, Mohd Cairul Iqbal, 2023. Poly (N-isopropylacrylamide)-based polymers: Recent overview for the development of temperature-responsive drug delivery and biomedical applications. Macromol. Chem. Phys. 224 (20), 2300157.
Shen, Qiming, Fang, Changhao, Serpe, Michael J., 2023. Microgel-based etalon immunoassay for IgG detection. Anal. Bioanal. Chem. 415 (23), 5645–5656.
Singh, Saumitra, Hasan, Mohd Rahil, Jain, Akshay, Pilloton, Roberto, Narang, Jagriti, 2023. LFA: the mysterious paper-based biosensor: a futuristic overview. Chemosensors 11 (4), 255.
Sorrell, Courtney D., Carter, Matthew C.D., Serpe, Michael J., 2011. A "paint-on" protocol for the facile assembly of uniform microgel coatings for color tunable etalon fabrication. ACS Appl. Mater. Interfaces 3 (4), 1140–1147.
Sorrell, Courtney D., Serpe, Michael J., 2012. Glucose sensitive poly (N-isopropylacrylamide) microgel based etalons. Anal. Bioanal. Chem. 402, 2385–2393.
Tang, Ruihua, Xie, Ming Yue, Li, Min, Cao, Lei, Feng, Shangsheng, Li, Zedong, Xu, Feng, 2022. Nitrocellulose membrane for paper-based biosensor. Appl. Mater. Today 26, 101305.
Van Tam, Tran, Hur, Seung Hyun, Chung, Jin Suk, Choi, Won Mook, 2021. Novel paper-and fiber optic-based fluorescent sensor for glucose detection using aniline-functionalized graphene quantum dots. Sensors Actuators B: Chem. 329, 129250.
Venetis, Christos A., Tarlatzis, Basil C., 2018. Trying to define the optimal progesterone elevation cut-off in fresh in vitro fertilization cycles: time to evolve our way of thinking. Fertil. Steril. 110 (4), 634–635.
Villena Gonzales, Wilbert, Mobashsher, Ahmed Toaha, Abbosh, Amin, 2019. The progress of glucose monitoring—A review of invasive to minimally and non-invasive techniques, devices and sensors. Sensors 19 (4), 800.
Wang, Jingying, Zhang, Xieli, Shi, Kaiyao, Zhang, Qiang, 2021. Optical devices constructed from responsive microgels for polyphenols detection. Front. Chem. 9, 580025.
Wei, Menglian, Li, Xue, Serpe, Michael J., 2019. Stimuli-responsive microgel-based surface plasmon resonance transducer for glucose detection using a competitive assay with concanavalin a. ACS Appl. Polym. Mater. 1 (3), 519–525.
Wen, Quan, Pelton, Robert, 2012. Design rules for microgel-supported adhesives. Ind. Eng. Chem. Res. 51 (28), 9564–9570.
Xuan, Hongyun, Ren, Jiaoyu, Zhu, Yanxi, Zhao, Bo, Ge, Liqin, 2016. Aptamer-functionalized P (NIPAM-AA) hydrogel fabricated one-dimensional photonic crystals (1DPCs) for colorimetric sensing. RSC Adv. 6 (43), 36827–36833.
Younes, Nadin, Yassine, Hadi M, Kourentzi, Katerina, Tang, Patrick, Litvinov, Dmitri, Willson, Richard C, Abu-Raddad, Laith J, Nasrallah, Gheyath K, 2023. A review of rapid food safety testing: using lateral flow assay platform to detect foodborne pathogens. Crit. Rev. Food Sci. Nutr. 64 (27), 9910–9932.
Zheng, Chujun, Wang, Kan, Zheng, Wei, Cheng, Yuemeng, Li, Tangan, Cao, Bo, Jin, Qinghui, Cui, Daxiang, 2021. Rapid developments in lateral flow immunoassay for nucleic acid detection. Analyst 146 (5), 1514–1528.
Zhou, Yaofeng, Wu, Yuhao, Ding, Lu, Huang, Xiaolin, Xiong, Yonghua, 2021. Point-of-care COVID-19 diagnostics powered by lateral flow assay. TRAC Trends Anal. Chem. 145, 116452.
Zhu, Guo-Dong, Yang, Cao-Ying, Yin, Yu-Rong, Yi, Zhuan, Chen, Xian-Hong, Liu, Li-Fen, Gao, Cong-Jie, 2019. Preparation of isoporous membranes from low χ block copolymers via co-assembly with H-bond interacting homopolymers. J. Membr. Sci. 589, 117255.